1

Dual-Band Aerial Networks for Priority-Based Traffic

Abdullah Ridwan Hossain, Graduate Student Member, IEEE, Mohammad Arif Hossain, Graduate Student Member, IEEE and Nirwan Ansari, Fellow, IEEE

Abstract-Unmanned aerial vehicle networks suffer from lackluster performance due to line-of-sight issues as well as resource scarcity. Network slicing, multi-band transmission, and numerology show great potential in mitigating such limitations. In this work, we propose the use of the sub-6 GHz and mmWave bands, the latter of which requires careful consideration of line-of-sight, with numerology for aerial network slicing to provision timecritical services and broadband access. Accordingly, we formulate a user admission control policy to regulate band access after which we formulate a joint resource block and power allocation problem, a mixed-integer non-linear programming problem, to minimize the quality-of-service gap of the throughput-dependent broadband users as a best-effort service and meet the time-critical service requirements. We propose a low-complexity algorithm, PREDICT, to tackle the formulated problem and present extensive simulation results to validate the advantages of our scheme.

Index Terms—admission control, best-effort, dual-band, resource allocation, mmWave, UAV.

I. INTRODUCTION

RECENTLY, unmanned aerial vehicle (UAV) networks have garnered significant attention in the research literature due to the UAVs' ease of deployment, size, and mobility, which enable them to enhance line-of-sight (LoS) communications to improve network throughput and reliability. While the advancement of research within this field is to be applauded, much remains yet to be harnessed, specifically, in terms of integrating 5G-enabling technologies such as artificial intelligence [1], network slicing, mmWave, carrier aggregation, numerology [2], [3], non-orthogonal multiple access (NOMA) schemes [4], [5], [6], and more. Although such technologies have great potential in minimizing such challenges, it is still quite ambitious to expect UAVs to provision throughput and time-sensitive services with maximum reliability perpetually.

Furthermore, while the integration of network slicing and dual-band transmission (sub-6 GHz and mmWave bands) with UAVs is a step in the right direction, it brings a new series of challenges to the forefront such as network security, energy and spectral efficiencies, aerial heterogeneity, massive multiple-input-multiple-output (MIMO) deployment, and so

Copyright (c) 2015 IEEE. Personal use of this material is permitted. However, permission to use this material for any other purposes must be obtained from the IEEE by sending a request to pubs-permissions@ieee.org.

This work was supported in part by the National Science Foundation under Grant CNS-1814748.

The authors are with the Advanced Networking Laboratory of the Department of Electrical and Computer Engineering, New Jersey Institute of Technology, Newark, NJ, 07102 USA. E-mail: {arh24, mh624, nirwan.ansari}@njit.edu.

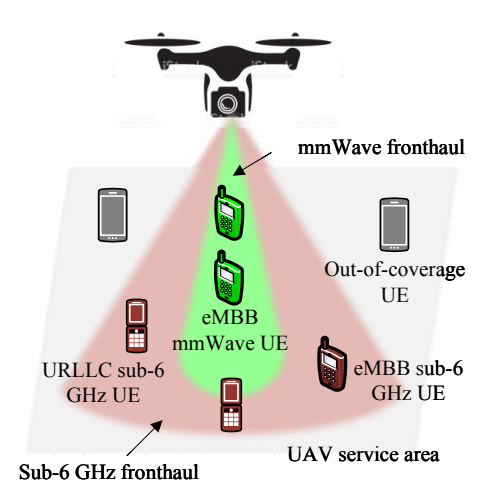


Fig. 1. Dual-band Numerology-enabled UAV network in a service area.

forth [7]. More specifically for dual-band aerial network scenarios though, there needs to be optimal policies to regulate a user equipment's (UE) band access. With the introduction of 5G numerology into the mix, numerology scheme selection is also a topic of study. The heterogeneous nature of the quality of service (QoS) requirements of the envisioned 5G use cases, namely, enhanced mobile broadband (eMBB), massive machine type communications (mMTC), and ultra-reliable low latency communications (URLLC), represent another hurdle [8].

Thus far, in the majority of UAV research literature, the common overarching theme is UAV placement or trajectory along with a single-band Long Term Evolution (LTE)-based resource allocation for the UEs [9], [10]. To the best of our knowledge, however, there has not been ample consideration of UAV networks where network slicing is involved over both the sub-6 GHz and mmWave bands in a numerologyenabled transmission scheme. With the dual-band transmission scheme, there is an additional need for the UAV to govern band access to the users of the slices. In other words, a robust channel and service-aware user access control (CSA-UAC) policy for the channel conditions, service types, channel bandwidths available across the different spectra, and more is imperative. mmWave transmissions themselves bring a set of unique challenges due to the extremely high frequencies and susceptibility to poor LoS conditions (this can be projected further to the use of THz transmissions for the envisioned 6G networks as well). 3GPP also standardized the novel new radio

(NR) numerology schemes which are expected to be utilized in the near future over both the sub-6 GHz and mmWave bands, formally referred to as frequency range 1 (FR1) and 2 (FR2), accordingly. The incorporation of 5G NR numerology schemes has been more or less limited to the ground networks only; their use has not been amply studied in aerial networks with network slicing despite their potentials in alleviating many of the well-known challenges of aerial networks. Moreover, there has been inadequate consideration of prioritized resource provisioning where the triaging of services needs to occur. Treating all service types identically is one of the defining hallmarks of the one-size-fits-all approach of legacy networks [11]. This is especially important because UAVs typically are endowed with merely a fraction of a ground base station's (gBS's) conventional transmit power.

Thus, a holistic approach is required where the resource allocation methodologies need to consider the available transmission spectra, total channel bandwidths, channel conditions, NR numerology schemes, and QoS requirements of the slices. These are vital factors that cannot be overlooked when assigning slices to the transmission bands and assigning wireless resources to the UEs. If such holistic considerations are instrumental for 5G ground networks, they would be even more so for 5G aerial networks. We can take it one step further and state that if such challenges loom over the 5G aerial networks, this would be far more the case for the envisioned 6G networks which seek to integrate terrestrial, aerial, low-earth-orbit, and subterranean networks along with THz transmissions. Hence, the results of the problem investigated in this work can potentially lay the ground work for future 6G considerations.

Accordingly, in this work, priority-based slicing is investigated where both non-critical and critical traffic contend with each other for resources over multiple bands with varying numerology schemes. Our contributions can be summarized as follows:

- We propose the deployment of a UAV equipped with dual-band transceivers for the fronthaul. The fronthaul utilizes both the sub-6 GHz and mmWave bands and supports all the 5G NR numerology schemes.
- We design a CSA-UAC policy to regulate the UEs' band access which is primarily dependent on their channel conditions, LoS, and slice request.
- 3) We formulate a joint power and resource allocation problem, a mixed integer non-linear programming (MINLP) problem, to minimize the provisioning gap of a best-effort throughput-dependent service while meeting the QoS requirements of a high-priority latency-sensitive service.
- 4) We propose our low-complexity algorithm, <u>PRiority BasED</u> Resource AllocatIon in Adaptive SliCed NeTwork (PREDICT) algorithm, which allocates the sub-6 GHz and mmWave band resource blocks after the UAC policy is executed, to efficiently solve the MINLP problem.
- 5) We discuss the extensive simulation results to validate our UAC policy and PREDICT; we benchmark the results against the LTE-based scenarios and suggest potential avenues of future research.

The rest of the paper is organized as follows. In Section II, we provide a short review of recent related works. In Section III, we present the downlink network model and formulate our CSA-UAC policy. In Section IV, we formulate the MINLP problem which is tackled efficiently by the proposed low-complexity PREDICT algorithm of Section V. Section VI offers simulation results, discussions, and analyses to validate our approach. Finally, in Section VII, we offer concluding remarks and present several avenues of future research for aerial networks.

II. RELATED WORKS

There have been extensive works already done in the field of UAV communications, especially related to its optimal placement as well as resource allocation. Sun et al. [12] investigated UAV placement and resource allocation strategies to minimize the latency experienced by the users within a hotspot. Al-Hourani et al. [13] derived the optimal UAV elevation which is dependent on the users' maximum pathloss thresholds and the radial coverage of the UAV. Alzenad et al. [14] maximized the number of served users by the UAV while minimizing the UAV transmission power. More recently, Yang et al. [15] utilized machine learning for user location prediction and channel estimation methods. Gui et al. [16] investigated the use of mmWave bands in UAV networks for wireless recharging and radio access service in a disaster area. Wu et al. [17] explored the numerous challenges with UAV communications and the provisioning of resources for different purposed slices for 5G. They specifically elaborated upon the challenges of incorporating massive-input-massive-output antennae, mmWave communications, and NOMA schemes in UAV networks. Hsu et al. [18] studied an IoT network which offloads tasks to the cloud servers utilizing both licensed and unlicensed 5G radio spectra. Their proposed algorithms successfully minimized the blocking probability and enhanced power savings and increased user throughputs. Weerasinghe et al. [19] studied grant-free resource allocations for mMTC traffic with dynamic time slot formats. Ansari et al. [20] proposed the use of free-space optics to provide both charging and backhaul functionalities for UAVs in order to alleviate the burden on the RF fronthaul while elongating the UAV's total flight time. Hossain et al. [21] proposed the allocation of numerology schemes at a highly granular level, on a per-device level in a mobile edge computing Internet-of-Things (IoT) network to maximize the flexibility in resource block tiling and network spectral efficiency while minimizing the energy consumption of the network and maintaining the deadlines of the offloaded tasks of the devices. Yin et al. [22] investigated user clustering, transmission power allocation, and content caching in a NOMA-based multi-UAV network via the ρ -K clustering and cross layer allocation methods; they took into consideration both the instantaneous and statistical QoS constraints to maximize the contents' hit probability while minimizing their outage probability. While the integration of optical communications into aerial networks is not a new phenomenon, Tadayyoni et al. [23] exploited the ultraviolet (UV) spectrum instead of the conventional optical wavelengths

to enable the collection of data from devices situated within an IoT farm; they studied the bit error rate (BER) and derived its closed-form expression which was then verified by simulations. Furthermore, they demonstrated that despite the leakage of UV transmission between one node to another, with the proper displacement choice between said nodes, the effect of interference is minimal and the performance of the system remains identical to that of the no-interference case.

While the recent works are quite impactful and have advanced the state of the art, there remains much to be explored. mmWave has been deployed experimentally on a growing scale across different settings and has become commercially available. For a UAV to truly indeed function as a transparent relay node between a gBS and UE, it must use RF bands similar to those of the gBS for optimal provisioning. 5G gBSs are expected to utilize the standardized numerology schemes to enhance throughput, power consumption, latency, etc. UAVs are expected to be operated as a transparent arm of 5G ground networks and as such, require to be equally robust in their resource provisioning and capabilities. This requires an indepth study into band access schemes for such aerial networks as well.

In ultra-dense networks, it is improbable to provision all UEs without any outages thus necessitating the need to triage UEs when allocating resources. Consequently, some best-effort UEs will experience a degraded quality-of-experience (QoE) due to a provisioning gap between the required QoS and what was allocated; such a QoS provisioning gap should be addressed especially in the light of the above factors which have not been considered in the research literature. Lastly, we consider the channel condition of each individual resource block (RB) as opposed to simplifying it to a single carrier frequency of the entire band as done in the majority of all other works. This gives us a much more realistic depiction of practical networks which must consider the frequencydependent channel gains on each RB of a wireless network for optimal wireless resource allocation. Although the effect of the per-RB dependency is negligible in the sub-6 GHz region, it is extremely pronounced in the mmWave band and greatly impacts the overall resource allocation. This impact is considered in our resource allocation scheme.

III. DOWNLINK NETWORK MODEL

In this section, we present our overall system model. Consider a UAV utilizing an orthogonal frequency division multiple access (OFDMA) scheme (Fig. 1). The UAV is equipped with sub-6 GHz and mmWave band transceivers for the fronthaul (the backhaul is not considered here) and support all the NR numerology schemes. The UEs are either throughput-sensitive (eMBB) or latency-sensitive (URLLC); the former is a best-effort service while the latter is a high-priority service. We note here that an mMTC slice can also be considered with the corresponding QoS constraints, but, for simplicity, we only consider the eMBB and URLLC slices (the mMTC service does not typically have sensitive requirements). The UAV will triage the two service types, meaning that the UAV must uphold full reliability for the

URLLC slice at all times no matter the overall condition of the network. Resultantly, the eMBB slice may experience a QoS provisioning gap. The UAV will assign each UE to one of two transmission bands based on its requested service type and channel condition (this mechanism is detailed in Section V). It is assumed that the number of RBs in the mmWave band is always greater than that of the sub-6 GHz band (the reasons as to why are clarified in Section VI).

A. Pathloss and Throughput Models

The pathloss model utilized in this work is probabilistic and dependent on primarily two factors: free space path loss (FSPL) and probability of line-of-sight (PLoS). We first determine the LoS pathloss, $PL_{u,n}^{LoS}$, between the UAV and UE u on RB n whose carrier frequency is f_n [24]:

$$PL_{u,n}^{LoS}(dB) = 20\log\left(\frac{4\pi f_n d_u}{c}\right) + \eta_{LoS},\tag{1}$$

where the first term is the FSPL and the second, η_{LoS} , is the additional average LoS link loss in dB. η_{LoS} depends on the environment where the network is situated, i.e., rural, suburban, urban, etc. d_u is the distance (in meters) between the UAV and UE u while c is the speed of light (meters per second). The non-line-of-sight (NLoS) pathloss can be determined as follows:

$$PL_{u,n}^{NLoS}(dB) = 20\log\left(\frac{4\pi f_n d_u}{c}\right) + \eta_{NLoS},\tag{2}$$

where the second term, η_{NLoS} , is the additional average NLoS link loss (in dB) which also depends on the environment i.e., rural, suburban, urban, etc. For example, the average loss values for (η_{LoS} , η_{NLoS}) would be (0.1, 21), (1.0, 20), (1.6, 23), and (2.3, 34), for suburban, urban, dense urban, and highrise urban environments, correspondingly [25]. Now that we have determined the path losses for the LoS and NLoS links, we need to determine the probabilities of occurrence for each type, PR_u^{LoS} and PR_u^{NLoS} , respectively [13]:

$$PR_u^{LoS} = \frac{1}{1 + a\exp(-b(\frac{180}{\pi}\theta_u - a))},$$
 (3)

$$PR_u^{NLoS} = 1 - PR_u^{LoS},\tag{4}$$

where a and b are environmental constants while θ_u is the elevation angle (in radians) of the UAV with respect to UE u. Therefore, the linearized LoS and NLoS channel gains can be determined from the logarithmic pathlosses (dB) respectively as follows [26]:

$$g_{u,n}^{LoS} = 10^{-\frac{PL_{u,n}^{LoS}(dB)}{10}},$$
 (5)

$$g_{u,n}^{NLoS} = 10^{-\frac{PL_{u,n}^{NLoS}(dB)}{10}}. (6)$$

The wireless throughput of the fronthaul for UE u over RB n, per the Shannon capacity is [27],

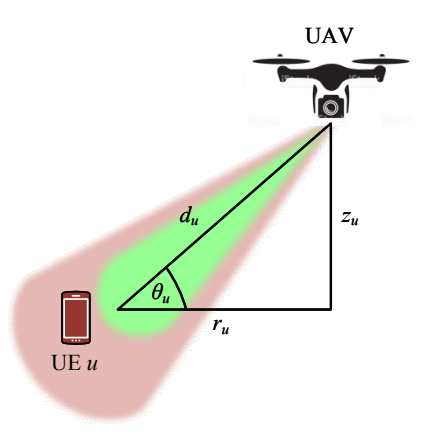


Fig. 2. UAV location with respect to a UE.

$$\begin{split} R_{n}^{u} &= B^{RB} \log_{2} \left(1 + \frac{g_{u,n}^{LoS} P_{n}^{u}}{B^{RB} N_{0}} \right) (PR_{u}^{LoS}) + \\ B^{RB} \log_{2} \left(1 + \frac{g_{u,n}^{NLoS} P_{n}^{u}}{B^{RB} N_{0}} \right) (PR_{u}^{NLoS}), \end{split} \tag{7}$$

where B^{RB} is the RB bandwidth (varies with numerology scheme), P_n^u is the UAV transmit power on RB n for UE u, and N_0 is the noise spectral density. Therefore, the total data rate of UE u over all its allocated RBs would be:

$$R_{u} = \sum_{n=1}^{|\mathcal{N}^{S}|} a_{n}^{u} R_{n}^{u}, \tag{8}$$

where a_n^u is a binary indicator variable to represent if RB n is allocated to UE u and \mathcal{N}^S is the set of RBs over the sub-6 GHz band. Fig. 2 portrays the UAV location with respect to a UE.

B. CSA-UAC Policy

We design our CSA-UAC policy in Algorithm 1 for the UEs to be assigned to either the sub-6 GHz or mmWave bands. The policy essentially assigns each individual UE to either the sub-6 GHz or mmWave bands after which the joint resource block and power allocation problem can be solved (discussed in the subsequent sections). The policy is dependent on the service type and PLoS of the UE. The PLoS of a UE is undoubtedly dependent on the UAV location. As the focus of this work is on the fronthaul resource allocation, the UAV placement problem is not formally addressed in this work; it is assumed that the UAV is already optimally placed within the hotspot such that it maximizes the throughput.

The mmWave band has its well-known challenges in terms of penetration, LoS, excessive attenuation, etc. [28], [29]. Since the URLLC slice does not generally require massive throughput, it does not need to employ mmWave links. As per Eqs. (1)-(2), it is clear that higher transmission frequencies lead to significantly higher path losses which do not bode well for sensitive traffic such as that of the URLLC slice. Moreover, a slight degradation in the mmWave LoS link will result in a much more pronounced deterioration of the channel

Algorithm 1: CSA-UAC Policy

```
Input: Unassociated eMBB and URLLC UEs
  Output: UE-Band assignments
1 for all UEs do
2
      if UE requests URLLC service type then
         assign UE to sub-6 GHz band
3
      end
4
5
         Calculate PLoS of UE
 6
7
         if PLoS of UE < PLoS Threshold then
             assign UE to sub-6 GHz band
 8
         end
10
             assign UE to mmWave band
11
         end
12
      end
13
14 end
```

gain than it would at the sub-6 GHz band. Therefore, to ensure maximum reliability and channel stability, our CSA-UAC policy places the URLLC slice exclusively on the sub-6 GHz band.

The eMBB slice does not have the same stringent requirements; hence, more liberties can be taken with its traffic. For each eMBB UE, if it is above a certain PLoS threshold, it is assigned to the mmWave band; otherwise, it is associated with the sub-6 GHz band instead. The tuning of this PLoS threshold greatly impacts the overall resource allocation of the slices as the simulation results in Section VI will demonstrate.

IV. PROBLEM FORMULATION

After the CSA-UAC policy is executed, the UAV must allocate bandwidth and transmission power to the users per their priority. Thus, we formulate a QoS gap minimization problem, which is a joint power and RB allocation problem, for the eMBB slice (best-effort). By design, the QoS gap in this work strictly refers to the throughput gap of the best-effort slice only.

A. Objective Function

The objective function seeks to minimize the average QoS degradation of the eMBB slice as follows,

$$\min_{\boldsymbol{A},\boldsymbol{B},\boldsymbol{C},\boldsymbol{J},\boldsymbol{P}^{S},\boldsymbol{P}^{M},\boldsymbol{Q}} \frac{1}{|\mathcal{U}_{E}^{S}| + |\mathcal{U}_{E}^{M}|} \left(\sum_{u=1}^{|\mathcal{U}_{E}^{S}|} Q_{u} + \sum_{v=1}^{|\mathcal{U}_{E}^{M}|} J_{v} \right). \quad (9)$$

We denote the sets of RBs for the sub-6 GHz and mmWave bands as \mathcal{N}^S and \mathcal{N}^M , respectively. The superscripts S and M serve to identify which band the RB set is from: S is for the sub-6 GHz band and M is for the mmWave band. Furthermore, we denote the set of eMBB UEs on the sub-6 GHz and mmWave bands as \mathcal{U}_E^S and \mathcal{U}_E^M , respectively. We define the following decision variables: $A = \{a_n^u\}$, $B = \{b_n^v\}$, and $C = \{c_n^w\}$ as RB allocation binary indicators. $P^S = \{P_{u,n}\}$ and $P^M = \{P_{v,m}\}$ are the power allocation variables per RB

n and m on each band for a band's UE u and v respectively. Q_u represents the QoS gap of eMBB UE u of the sub-6 GHz band while J_v represents the same for the mmWave eMBB UEs. They are written as decision variables in matrix form, J and Q.

Prior to defining the constraints of the system, we need to define the achieved throughput of each UE. In an ideal scenario where the network can always accommodate the needs of all its UEs, the UEs would be meeting all their QoS requirements. However, in a heavily-loaded network, this is highly improbable to achieve and as such, the resource allocation process will have to prioritize certain UEs over others. It follows that the UEs' achieved throughputs would simply be the difference between their required and actually achieved throughputs:

$$Q_u = D_E - R_u, \forall u \in \mathcal{U}_E^S, \tag{10}$$

$$J_{v} = D_{E} - R_{v}, \forall v \in \mathcal{U}_{E}^{M}, \tag{11}$$

where R_u (and by extension, R_v) is obtained from Eq. (8) and D_E denotes the eMBB slice's minimum required throughput.

B. Constraints

We can now proceed to define our system constraints:

 Maximum Transmission Power: The UAV has a limited transmission power per band. Therefore, the transmission power constraint can be formulated as follows:

$$P_{u,n}^{S} \le \frac{P_{UAV}^{S}}{|\mathcal{N}^{S}|}, \forall u \in \mathcal{U}^{S}, \ \forall n \in \mathcal{N}^{S},$$
 (12)

$$P_{v,m}^{M} \le \frac{P_{UAV}^{M}}{|\mathcal{N}^{M}|}, \forall v \in \mathcal{U}^{M}, \ \forall m \in \mathcal{N}^{M},$$
 (13)

where the maximum transmit power of the UAV on each respective band is denoted by P_{UAV}^S and P_{UAV}^M , respectively. $P_{u,n}^S$ is the transmit power of the UAV over RB n of UE u over the sub-6 GHz band while $P_{v,m}^M$ is the transmit power of the UAV over RB m of user v over the mmWave band.

2) Total Channel Bandwidth: The allocated bandwidth cannot exceed the total channel bandwidth available (total number of RBs available) in each band:

$$\sum_{u=1}^{|\mathcal{U}_{E}^{S}|} \sum_{n=1}^{|\mathcal{N}^{S}|} a_{n}^{u} + \sum_{w=1}^{|\mathcal{U}_{U}|} \sum_{n=1}^{|\mathcal{N}^{S}|} c_{n}^{w} \le |\mathcal{N}^{S}|, \tag{14}$$

$$\sum_{v=1}^{|\mathcal{U}_{E}^{M}|} \sum_{m=1}^{|\mathcal{N}^{M}|} b_{m}^{v} \le |\mathcal{N}^{M}|.$$
 (15)

3) Orthogonal Wireless Access: We ensure that each allocated RB in both bands is utilized by one user at most:

$$\sum_{u=1}^{|\mathcal{U}_{E}^{u}|} a_{n}^{u} + \sum_{w=1}^{|\mathcal{U}_{U}|} c_{n}^{w} \le 1, \forall n \in \mathcal{N}^{S}, \tag{16}$$

$$\sum_{v=1}^{|\mathcal{U}_E^M|} b_m^v \le 1, \forall m \in \mathcal{N}^M.$$
 (17)

4) Binary Indicators: We enforce the integral nature of the binary RB association indicators by the following constraints:

$$a_n^u \in \{0, 1\}, \forall u \in \mathcal{U}_F^S, \forall n \in \mathcal{N}^S,$$
 (18)

$$b_m^v \in \{0, 1\}, \forall v \in \mathcal{U}_E^M, \forall m \in \mathcal{N}^M,$$
 (19)

$$c_n^w \in \{0, 1\}, \forall w \in \mathcal{U}_U, \forall n \in \mathcal{N}^S.$$
 (20)

 a_n^u denotes if RB n of the sub-6 GHz band, \mathcal{N}^S , is allocated to UE u of the eMBB slice, \mathcal{U}_E^S . b_m^v denotes if RB m of the mmWave band, \mathcal{N}^M , is allocated to user v of the eMBB slice, \mathcal{U}_E^M . Lastly, c_n^w denotes if RB n of the sub-6 GHz band, \mathcal{N}^S , is allocated to user w of the URLLC slice, \mathcal{U}_U . These are all written in matrix form in the objective function.

5) URLLC Latency: The network must meet the per-bit transmission latency requirement, T, of the URLLC slice. The achieved latency of UE w of the URLLC slice, denoted by τ_w (ms/b), should satisfy the following constraint:

$$\tau_w \le T, \forall w \in \mathcal{U}_U,$$
(21)

where

$$\tau_w = \frac{1}{R_w} \tag{22}$$

Note that the URLLC UEs, denoted by the set \mathcal{U}_U , are always granted the slice's minimum required QoS. The URLLC service is the most stringent of all, and thus does not tolerate any QoS gaps. As this slice always utilizes the sub-6 GHz band, there is no need for a superscript S (unlike the sets of eMBB UEs).

Thus, the MINLP problem can be written as P1 below:

P1:
$$\min_{A,B,C,J,P^S,P^M,Q} \frac{1}{|\mathcal{U}_E^S| + |\mathcal{U}_E^M|} \left(\sum_{u=1}^{|\mathcal{U}_E^S|} Q_u + \sum_{v=1}^{|\mathcal{U}_E^M|} J_v \right)$$
s.t. (12) - (21).

We would like to bring the reader's attention to the primary decision variables **J** and **Q**. There are three possible cases and respective implications to consider in their regard:

- 1) Q_u (or J_v) is positive: indicates that a user's throughput is below D_E ,
- 2) Q_u (or J_v) is zero: indicates that a user's throughput is equal to D_E ,
- 3) Q_u (or J_v) is negative: indicates that a user's throughput is above D_F .

Minimizing the average QoS degradation as per Eq. (9) implies the maximization of its negative value which is equivalent to minimizing its positive value. To minimize its positive value, the network will seek to maximize the average throughput of the network. We can then conclude that minimizing the average QoS gap of the network is equivalent to, both in meaning and mathematically, maximizing the average throughput of the

network. Accordingly, we use the phrases average throughput maximization and average QoS gap (or degradation) minimization, interchangeably.

V. DUAL-BAND RESOURCE ALLOCATION POLICY: PREDICT

To solve P1 which is evidently an MINLP problem, we propose the PRiority BasED Resource AllocatIon in Adaptive SliCed NeTwork (PREDICT) algorithm which is to be executed after the CSA-UAC policy is applied. PREDICT (Algorithm 2) works in the following fashion: first, it calculates the channel gains of each UE on each band's RBs (Line 1). Subsequently, as per Line 2, the UAV allocates its maximum transmission power on each of the RBs as dictated by Eqs. (12)-(13) so that each UE's data rate per RB can be calculated in Line 3 via Eq. (7). The UEs of all slices on all the bands are then sorted from the best channel conditions to the worst (Line 4). The URLLC UEs are provisioned RBs first due to their high-priority status. For each URLLC UE, the RBs are sorted from the lowest-throughput RBs to the highest-throughput RB (Line 5). A URLLC UE is allocated RBs sequentially from the lowest-throughput RB to the highest-throughput RB in that order until its latency requirements are met (Line 8). These allocated RBs are removed from the sub-6 GHz RB set (Line 9). This is repeated for each URLLC UE until they are all satisfied (Lines 6-12).

Next, the eMBB UEs on both bands are assigned to RBs; arbitrarily, we start with the sub-6 GHz band. For each eMBB UE, the RBs are sorted from the highest-throughput RBs to the lowest-throughput RBs (Line 12). Each eMBB UE is allocated RBs sequentially from the lowest-throughput RBs to the highest-throughput RBs in that order, until its minimum throughput is met or there are no RBs left on that band; the allocated RBs are removed from the sub-6 GHz RB set (Lines 13-18). The same process is repeated for the mmWave band eMBB UEs. Finally, as for the surplus RB allocation for the eMBB UEs in Lines 19-22, if there are any remaining RBs which have yet to be allocated, on either band, they are to be allocated to the single UE that achieves the highest throughput on those RBs in order to minimize Eq. (9).

A. Complexity Analysis

We now present the complexity analysis of PREDICT.

- The complexities of sorting $|\mathcal{U}_{\mathcal{E}}^{\mathcal{S}}|$, $|\mathcal{U}_{\mathcal{E}}^{\mathcal{M}}|$, and $|\mathcal{U}_{U}|$ UEs, are $O(|\mathcal{U}_{\mathcal{E}}^{\mathcal{S}}|\log|\mathcal{U}_{\mathcal{E}}^{\mathcal{S}}|)$, $O(|\mathcal{U}_{\mathcal{E}}^{\mathcal{S}}|\log|\mathcal{U}_{\mathcal{E}}^{\mathcal{S}}|)$, and $O(|\mathcal{U}_{U}|\log|\mathcal{U}_{U}|)$, respectively (Line 4).
- The complexities of sorting $|\mathcal{N}^S|$ RBs of the sub-6 GHz band for the URLLC UEs is $O(|\mathcal{N}^S| \log |\mathcal{N}^S|)$ (Line 5).
- Sub-6 GHz RB allocation for URLLC slice: The complexity of allocating the sub-6 GHz RBs, $|\mathcal{N}^S|$, to the URLLC UEs is $O(|\mathcal{N}^S|(|\mathcal{N}^S|-1)/2)$ which can be simplified to $O(|\mathcal{N}^S|^2)$ (Lines 6-11).
- The complexities of sorting the remaining $|\mathcal{N}^S |\mathcal{U}_U||$ sub-6 GHz RBs and $|\mathcal{N}^M|$ mmWave RBs for the eMBB UEs are $O((|\mathcal{N}^S| |\mathcal{U}_U|)\log(|\mathcal{N}^S| |\mathcal{U}_U|))$ and $O(|\mathcal{N}^M|\log|\mathcal{N}^S|)$, respectively (Line 13).

Algorithm 2: PREDICT Algorithm

Input: UE band associations, network parameters **Output:** UE RB assignments, QoS degradation

- 1 Calculate the LoS and NLoS channel gains $(g_{u,n}^{LoS})$ and $g_{u,n}^{NLoS}$ as per Eqs. (5)-(6)
- 2 Allocate the maximum transmit power available $(P_n^S \text{ and } P_n^M)$ to each RB as per Eqs. (12)-(13)
- 3 Calculate the throughput (R_n^u) per UE on each RB as per Eq. (7)
- 4 Sequence the UEs from the best channel gains to the worst

Sub-6 GHz RB allocation for URLLC UEs:

- 5 For each UE, sequence the RBs from the lowest throughput to the highest
- 6 for w = 1 to $|\mathcal{U}_U|$ do 7 | while UE w is not satisfied do

assign the RBs from the lowest to the highest throughput per RB consecutively and

orthogonally (Eq. (16)) until UE w's achieved per-bit latency satisfies Eq. (21)

Set the binary indicator in Eq. (20) equal to 1 Remove the allocated RBs from N^S

11 end

12 end

10

16

17

18

19

Repeat the following on both bands

Baseline RB allocation for eMBB UEs:

- 13 For each UE, sequence the RBs from the lowest throughput to the highest
- 14 for u = 1 to $|\mathcal{U}_E^S|$ do

while RBs are available (Eqs. (14)-(15)) && UE u is not satisfied do

assign the RBs from the lowest to the highest throughput per RB consecutively and orthogonally (Eq. (16) for sub-6 GHz and Eq. (17) for mmWave bands, respectively) until UE u's achieved data rate, R_u , is at least D_E . Set the binary indicators in Eq. (18) for sub-6 CHz argulate 1 (do the same for Eq. (10))

GHz equal to 1 (do the same for Eq. (19) when on mmWave band)

Remove the allocated RBs from \mathcal{N}^S

end

20 end

Surplus RB allocation for eMBB UEs:

- 21 while surplus RBs available (Eq. (16)) && all eMBB UEs are satisfied do
- Allocate the remaining RBs in N^S to the UE with highest throughput per RB
- Set the binary indicators in Eq. (18) for sub-6 GHz equal to 1 (do the same for Eq. (19) when on mmWave band)
- Remove the allocated RBs from \mathcal{N}^S

25 end

• Baseline RB allocation for eMBB slice on both bands: Similar to that of Lines 6-11, the complexities of allocating $(|\mathcal{N}^S| - |\mathcal{U}_U|)$ remaining sub-6 GHz band RBs and

TABLE I SIMULATION PARAMETERS

Parameter	Value
eMBB users	40
URLLC users	25
URLLC air-interface per-bit latency	0.5 ms/bit [30]
Sub-6 GHz carrier frequency	2.4 GHz
mmWave carrier frequency	25 GHz
Sub-6 GHz channel bandwidth	20 MHz
mmWave channel bandwidth	80 MHz
Maximum UAV transmission power	40 dBm
Noise spectral density	-174 dBm/Hz
sub-6 GHz numerology scheme	2
mmWave numerology scheme	5
Environmental constants (a, b)	9.61, 0.16 [13]
Average LoS and NLoS attenuation	1, 20 dB [13]
Hotspot size	60m × 60m

 $|\mathcal{N}^M|$ remaining mmWave band RBs to the eMBB UEs are $O(|\mathcal{N}^S| - |\mathcal{U}_U|)^2$ and $O(|\mathcal{N}^M|^2)$, respectively (Lines 14-20).

The overall complexity of PREDICT algorithm can be written as: $O(|\mathcal{U}_{\mathcal{E}}^{S}|\log|\mathcal{U}_{\mathcal{E}}^{S}|+|\mathcal{U}_{\mathcal{E}}^{S}|\log|\mathcal{U}_{\mathcal{E}}^{S}|+|\mathcal{U}_{U}|\log|\mathcal{U}_{U}|+|\mathcal{N}^{S}|\log|\mathcal{N}^{S}|+|\mathcal{N}^{S}|^{2}+(|\mathcal{N}^{S}|-|\mathcal{U}_{U}|)\log(|\mathcal{N}^{S}|-|\mathcal{U}_{U}|)+|\mathcal{N}^{M}|\log|\mathcal{N}^{S}|+(|\mathcal{N}^{S}|-|\mathcal{U}_{U}|)^{2}+|\mathcal{N}^{M}|^{2}.$ As $|\mathcal{N}^{S}|\geq|\mathcal{U}_{\mathcal{E}}^{S}|,$ $|\mathcal{N}^{S}|\geq|\mathcal{U}_{\mathcal{E}}^{S}|,$ $|\mathcal{N}^{S}|\geq|\mathcal{U}_{\mathcal{E}}^{M}|,$ $|\mathcal{N}^{S}|\geq|\mathcal{U}_{U}|,$ and $|\mathcal{N}^{M}|>|\mathcal{N}^{S}|,$ we can then simplify the overall complexity of PREDICT and write it as: $O(|\mathcal{N}^{M}|\log|\mathcal{N}^{M}|+|\mathcal{N}^{M}|^{2}).$ We can then further simplify the complexity as it tends to $O(|\mathcal{N}^{M}|^{2}).$

VI. SIMULATIONS AND DISCUSSION

We now present an in-depth discussion of our simulation results. Table I summarizes the fixed simulation parameters utilized for this work. All the generated data points in the simulation figures are averaged over 500 Monte Carlo simulations. Most of the simulation results only display the eMBB slice's performance because the URLLC traffic is always satisfied. We investigate the performance of our network under five different cases:

- Varying the minimum eMBB throughput requirements and probability threshold (for user admission into the mmWave band),
- 2) Varying eMBB user load, throughput requirement, and said probability threshold,
- 3) Varying the total channel bandwidth,
- 4) Varying numerology schemes of both bands, and
- 5) Legacy vs dual-band numerology-enabled aerial network performance comparison.

A. Varying eMBB Throughput Requirement and Probability Threshold

In this section, we investigate the eMBB slice's performance with varying probability thresholds and throughput requirements. Here, we bring to the reader's attention that since the maximum bandwidth allowed in 4G-LTE networks is 20 MHz only, we deemed it appropriate to utilize this amount as the minimum bandwidth for the sub-6 GHz band in our 5G UAV network. Furthermore, because the maximum bandwidth

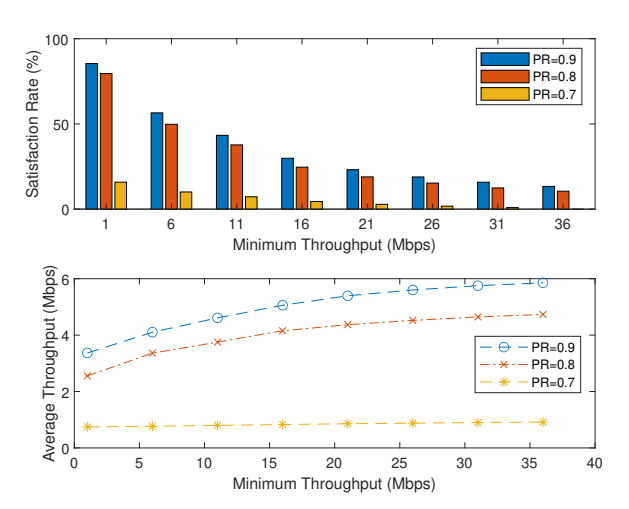


Fig. 3. eMBB performance under increasing throughput requirements. "PR" represents the threshold probability of the mmWave band admission in the CSA-UAC policy.

available for 5G networks at the sub-6 GHz band is 100 MHz while that of the mmWave band is 400 MHz, the 5G aerial networks in our simulation scenarios always maintain a 1-to-4 channel bandwidth ratio between said bands and hence, we only explicitly mention the sub-6 GHz bandwidth in the results since it is implied that the mmWave bandwidth is four times that amount by default.

Fig. 3 makes clear that lowering the PLoS threshold in the CSA-UAC policy incurs higher QoS gaps, and thus, lower satisfaction rates, for the eMBB slice overall; the satisfaction rate is the percentage of UEs that meet their minimum requirement. In the case of the eMBB slice, it is much higher only when the users with near-perfect PLoSs are admitted into the mmWave band. Lowering this threshold leads to a higher dissatisfaction of the slice due to an increasing number of users with poorer channel conditions being admitted into the mmWave band, thus making it more difficult for the UAV to satisfy their requirements. Even a slight decrease in the PLoS threshold results in a massive dissatisfaction of the slice. Users that would have been better served by the sub-6 GHz band are now instead assigned to the mmWave band. We also see that increasing the minimum required throughput of the eMBB slice further strains the UAV network. The pathloss at the mmWave band is much higher due to the high carrier frequencies of the mmWave RBs. Consequently, a slight decrease in LoS conditions at the mmWave band has a severe negative impact on the eMBB slice's performance.

Counter-intuitively, while the satisfaction rate worsens at higher requirements, the average throughput improves. The average throughput is actually driven by the UEs that can meet the higher throughput requirements; the higher the throughput that they can achieve, the higher the average throughput that is obtained. However, the average throughput curve eventually levels off because the UAV will exhaust all its resources and no longer be able to further increase any UE's throughput. The results for lower PLoS thresholds (below 0.7) are not shown since the network performance degrades too far.

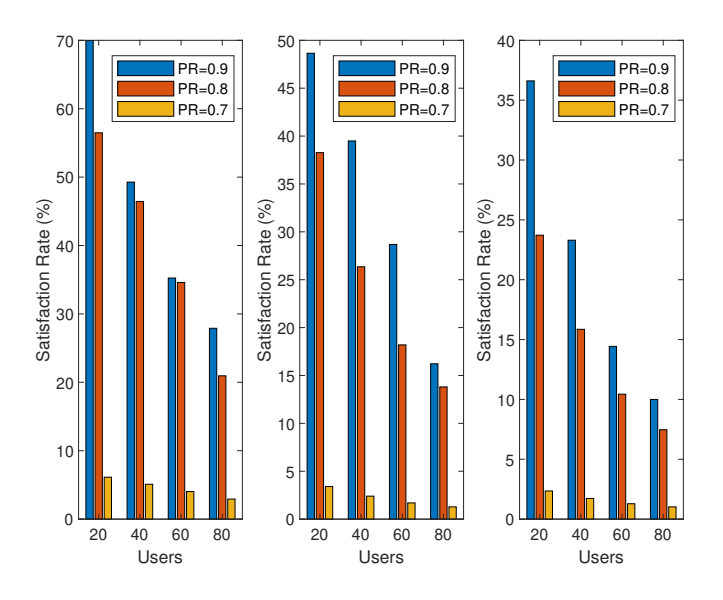


Fig. 4. eMBB performance under increasing user volumes at minimum throughput requirements of 5 Mbps (left), 10 Mbps (center), and 15 Mbps (right). "PR" represents the threshold probability of the mmWave band admission in the CSA-UAC policy.

B. Varying eMBB User Density

In Fig. 4, we assess the performance of the network under increased user loads at various throughput requirements, specifically at minimum requirements of 5, 10, and 15 Mbps. We see that as the minimum throughput requirement increases, even at a very high PLoS threshold, the network struggles to satisfy many of the users of the slice. The satisfaction of the slice suffers when the number of users in the eMBB slice increases; this is due to swift bandwidth exhaustion. This bandwidth exhaustion is brought on even faster at lower PLoS thresholds because more RBs are required to compensate for the lack of a strong LoS channel in the mmWave band. This further highlights the sensitivity of the mmWave band to LoS communication channels and underscores the need for a very stringent CSA-UAC policy.

C. Varying Channel Bandwidth

In Fig. 5, we examine how the network responds to bandwidth availability. We investigate the performance for a 15 Mbps minimum eMBB throughput. The addition of bandwidth affords more RBs for allocation which increases the satisfaction and average throughput of the slice. However, at a high enough amount of bandwidth, the satisfaction rate will level off because with the addition of more RBs, the transmission power per RB will gradually decrease so much so that the throughput on each RB, as dictated by Eq. (7), will be too little for it to be able to satisfy any UE. Therefore, increasing the channel bandwidth is not always favorable, especially for a UAV network (which already has limited transmission power). However, to offset the degraded performance at excessive channel bandwidths caused by the noise power, the UAV should be endowed with a higher transmission power to be able to allocate it over the added RBs without being spread out too

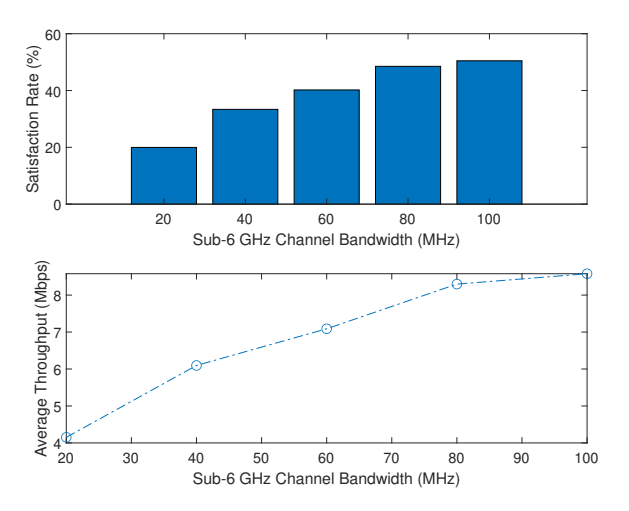


Fig. 5. eMBB performance with respect to bandwidth. The mmWave bandwidth (not shown explicitly) is four times that of the sub-6 GHz band and increases proportionally.

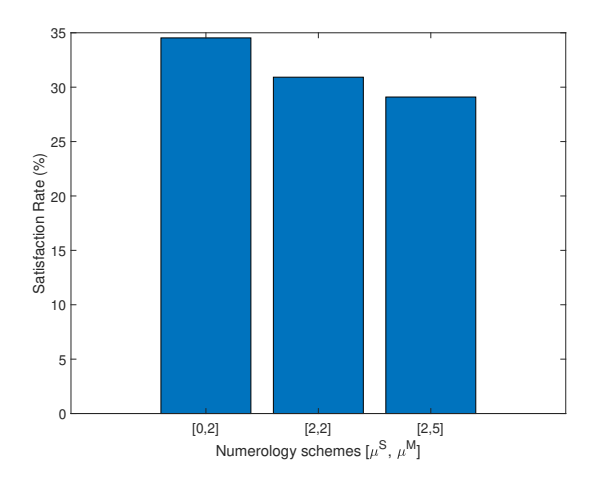


Fig. 6. eMBB performance with respect to numerology scheme.

thin. This is projected to be possible in the near future with the latest advancements in antenna design and UAV-related hardware.

D. Varying Numerology Schemes

In Fig. 6, we investigate the eMBB slice's performance for varying numerology schemes for a 10 Mbps minimum requirement. Surprisingly, it is shown that the lowest pair of numerology schemes outperform the highest. It is deducible that the higher numerology schemes, while increasing the RB bandwidth, also increase the associated noise of the RB. Furthermore, at lower numerology schemes, there are more RBs available for allocation to the UEs and hence it is easier to satisfy more users. Higher schemes generally mean fewer RBs available for allocation. Furthermore, those fewer available RBs have a much higher noise factor; without additional transmission power to overcome the noise, the RB's signal-to-interference-plus-noise ratio (SINR) degrades, thus lowering its throughput. Therefore, the eMBB slice is even

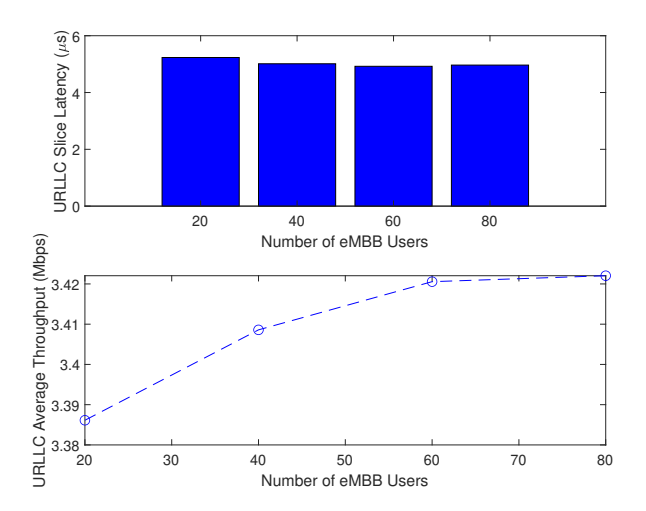


Fig. 7. URLLC performance with respect to eMBB user loads.

more sensitive to the PLoS thresholds at higher schemes. In other words, at the higher numerology schemes, there is a much lower tolerance for poor LoS conditions for users.

E. URLLC Performance Under Varying eMBB User Loads

In Fig. 7, we investigate the URLLC slice's performance for varying numerology schemes for a 10 Mbps minimum eMBB throughput. We see that despite the increasing load on the eMBB slice, the URLLC slice is able to maintain its requirements comfortably. The worst case latency is slightly greater than 5 μ s. Therefore, we have shown the resilience of the high-priority URLLC slice to poor performance despite the increasing load and/or poor channel conditions of the other heavily-loaded slices in the network. This is important since the URLLC slice is time-critical, has the highest priority in the network as per our system model, and requires the most effective slicing isolation.

F. Benchmarking PREDICT

In this section, we compare the performance of the legacy LTE scheme with PREDICT to validate the latter's advantages. Before doing so, we must note two inherent major differences between the two: firstly, in the legacy scheme, there is no need for a CSA-UAC policy since there is only a single transmission band (sub-6 GHz). Secondly, the RBs have a static bandwidth of 180 kHz only (which is equivalent to numerology scheme 0 of 5G networks) whereas in PREDICT, the RBs have wider bandwidths due to their numerology schemes. Along with other differences which are out of the scope of this work, these will impact and inform our analyses of the benchmark.

We now outline the simulation settings for this benchmark. The sub-6 GHz channel bandwidth for both the legacy LTE scheme and PREDICT is set to 20 MHz; the mmWave bandwidth in PREDICT is set to 80 MHz. Next, in accordance to the performance observed in Fig. 6, we set the numerology schemes under PREDICT to $\mu_S = 0$, $\mu_M = 2$. The legacy LTE network is set to scheme 0. The data rate of the eMBB slice

is set to 5 Mbps; the URLLC slice latency requirement is the same as in the previous scenarios (0.5 ms/bit) and its load is fixed to 25 users. As for the eMBB slice load, we vary it to demonstrate the performance difference between the legacy LTE scheme and PREDICT.

In Fig. 8, it is observed that the legacy scheme performs nearly identically as PREDICT at a minimum eMBB load; since both intra-slice (users within the same slice) and interslice (between different slices) contentions are negligible, both the legacy scheme and PREDICT have similar performances. However, there is indeed a slight performance lag of the legacy scheme at lower loads due to the static RB bandwidth (PREDICT allocates RBs of much higher bandwidths affording higher SINR and resilience to poorer LoS). We notice that the performance advantages of PREDICT under a stringent UAC policy, i.e., LoS threshold ≥ 0.8 , become more pronounced as the eMBB slice load increases. This is explicitly due to the increasing contention, smaller RB bandwidth, and smaller channel bandwidth of the LTE network. Additionally, PREDICT assigns users to the mmWave band and thus is better at alleviating contention whereas the legacy scheme has only the sub-6 GHz band to work with and is limited to 20 MHz.

Although PREDICT's performance does degrade as the network load increases, it always outperforms the legacy scheme with the exception of when the LoS threshold ≤ 0.7 . Recall that as the LoS threshold decreases, more users with poorer LoS conditions are admitted into the mmWave band. The mmWave band is highly sensitive to blockage especially in urban settings (η_{NLoS} =20 dB [13]). The throughput obtained on each RB for a user is extremely low and it makes it difficult for PREDICT to allocate enough RBs to meet its requirement thus allowing the legacy scheme to pull ahead. This underscores the great care that needs to be taken in designing a UAC policy when dual-band numerology-based UAVs are deployed. Essentially, there is a delicate balance between dual-band transmission, channel bandwidth and conditions, and numerology schemes in 5G aerial networks.

In traditional UAV communication schemes, a single wireless center frequency is assumed (around 2.4 GHz) for the channel modeling. In other words, the throughput for each RB on the sub-6 GHz band is calculated out to be identical and it only becomes a question of how many RBs (for integral constraints) or how much bandwidth (for continuous constraints) should be assigned to a UE. While this may be acceptable for approximate models in the sub-6 GHz region which can utilize up to 100 MHz channel bandwidths without carrier aggregation, strictly speaking however, this assumption significantly degrades the network performance when operating in the mmWave region. This is because even a slight increase in mmWave channel frequency massively worsens the resulting channel condition, and hence, the throughput on that RB. Moreover, up to 400 MHz bandwidth can be utilized without carrier aggregation at the mmWave region. Over this very large channel bandwidth, calculating a channel gain on one center frequency and applying the resulting throughput to the entire set of RBs will not work; the throughput of RBs at opposite ends of the channel bandwidth will have much disparity. Our proposed scheme adjusts for all such complications by

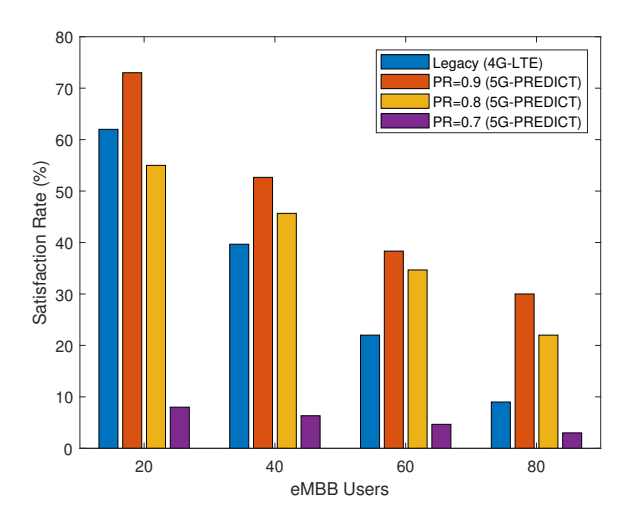


Fig. 8. Legacy and 5G numerology-enabled dual-band aerial network performances compared. "PR" represents the threshold probability of the mmWave band admission in the CSA-UAC policy.

calculating the channel condition and throughput on every RB on each band for each slice prior to determining the band-UE associations and transmit power allocations. This is one of catalysts behind PREDICT's superior performance.

Looking ahead to 6G networks which envision employing THz frequencies, such considerations will be even more imperative when modeling aerial-to-ground communication channels; PREDICT lays the groundwork for a more realistic implementation going ahead while incorporating numerology. Comparatively speaking, aerial-to-ground channels are much more susceptible to blockage than are ground-to-ground channels. Numerology does not negatively impact the resource allocation for ground-to-ground channels as much in mmWave bands, but this cannot be said for aerial networks for both mmWave and THz bands; our results have made that amply clear. We would further posit that aerial networks are more tolerant of sub-optimal UAV placements when not only utilizing dual-band schemes but also the 5G numerology schemes because the higher RB bandwidths can compensate for lower channel conditions to a certain extent. Furthermore, they also enable shorter time slots vital for URLLC use cases.

VII. CONCLUSION

We have combined network slicing and the novel numerology schemes within the sub-6 GHz and mmWave transmission spectra to demonstrate how a UAV must adopt a CSA-UAC policy and triage differing priorities of services to optimally allocate network resources. Furthermore, we observed the direct impact of PLoS on a best-effort service's satisfaction and throughput. We efficiently solved the proposed MINLP problem through our PREDICT algorithm to minimize the average QoS gap of the eMBB slice while maintaining full reliability of the URLLC slice. The results show that high network satisfaction is achievable with very stringent PLoS requirements even under strenuous conditions with the proper selection of the numerology scheme and transmission band. Furthermore, our proposed algorithm demonstrated superior

performance against the conventional UAV scheme. Throughout our discussions of the network performance, whether it be from the perspective of throughput, latency, or satisfaction rate, it becomes clear that our scheme strategically exploits the flexibility in RB bandwidth, mmWave band, as well as the increased channel bandwidth in that region, to mitigate the LoS challenges which are dominant in aerial-to-ground communication systems. We suggest that future areas of research should integrate coordinated multi-point support, carrier aggregation, and THz support for even more robust aerial network slicing because the simultaneous integration of these three technologies can unlock far more significant performance improvements for aerial network users.

REFERENCES

- M. A. Hossain, A. R. Hossain, and N. Ansari, "AI in 6G: Energyefficient distributed machine learning for multilayer heterogenous networks," *IEEE Network*, pp. 1–8, 2022.
- [2] A. Hossain and N. Ansari, "5G multi-band numerology-based TDD RAN slicing for throughput and latency sensitive services," *IEEE Transactions on Mobile Computing*, pp. 1–1, 2021.
- [3] Z. Xiao, P. Xia, and X.-g. Xia, "Enabling UAV cellular with millimeterwave communication: potentials and approaches," *IEEE Communica*tions Magazine, vol. 54, no. 5, pp. 66–73, 2016.
- [4] M. A. Hossain and N. Ansari, "Energy aware latency minimization for network slicing enabled edge computing," *IEEE Transactions on Green Communications and Networking*, vol. 5, no. 4, pp. 2150–2159, 2021.
- [5] E. N. Tominaga, H. Alves, O. L. A. López, R. D. Souza, J. L. Rebelatto, and M. Latva-aho, "Network slicing for eMBB and mMTC with NOMA and space diversity reception," in 2021 IEEE 93rd Vehicular Technology Conference (VTC2021-Spring), 2021, pp. 1–6.
- [6] M. A. Hossain and N. Ansari, "Network slicing for NOMA-enabled edge computing," *IEEE Transactions on Cloud Computing*, pp. 1–1, 2021.
- [7] Y. Xu, G. Gui, H. Gacanin, and F. Adachi, "A survey on resource allocation for 5G heterogeneous networks: Current research, future trends, and challenges," *IEEE Communications Surveys and Tutorials*, vol. 23, no. 2, pp. 668–695, 2021.
- [8] M. A. Hossain and N. Ansari, "Hybrid multiple access for network slicing aware mobile edge computing," *IEEE Transactions on Cloud Computing*, 2023, DOI:10.1109/TCC.2023.3234543, Early Access.
- [9] Q. Zhang, W. Saad, M. Bennis, X. Lu, M. Debbah, and W. Zuo, "Predictive deployment of UAV base stations in wireless networks: Machine learning meets contract theory," *IEEE Transactions on Wireless Communications*, vol. 20, no. 1, pp. 637–652, 2021.
- [10] X. Liu, Y. Liu, and Y. Chen, "Reinforcement learning in multiple-UAV networks: Deployment and movement design," *IEEE Transactions on Vehicular Technology*, vol. 68, no. 8, pp. 8036–8049, 2019.
- [11] A. R. Hossain and N. Ansari, "Priority-based downlink wireless resource provisioning for radio access network slicing," *IEEE Transactions on Vehicular Technology*, vol. 70, no. 9, pp. 9273–9281, 2021.
- [12] X. Sun, N. Ansari, and R. Fierro, "Jointly optimized 3D drone mounted base station deployment and user association in drone assisted mobile access networks," *IEEE Transactions on Vehicular Technology*, vol. 69, no. 2, pp. 2195–2203, 2020.
- [13] A. Al-Hourani, S. Kandeepan, and S. Lardner, "Optimal LAP altitude for maximum coverage," *IEEE Wireless Communications Letters*, vol. 3, no. 6, pp. 569–572, 2014.
- [14] M. Alzenad, A. El-Keyi, F. Lagum, and H. Yanikomeroglu, "3-D placement of an unmanned aerial vehicle base station (UAV-BS) for energy-efficient maximal coverage," *IEEE Wireless Communications Letters*, vol. 6, no. 4, pp. 434–437, 2017.
- [15] P. Yang, X. Xi, K. Guo, T. Q. S. Quek, J. Chen, and X. Cao, "Proactive UAV network slicing for URLLC and mobile broadband service multiplexing," *IEEE Journal on Selected Areas in Communications*, pp. 1–1, 2021.
- [16] J. Gui, N. Jin, and X. Deng, "Performance optimization in UAV-Assisted wireless powered mmWave networks for emergency communications," Wireless Communications and Mobile Computing, vol. 2021, p. 9936837, Jun 2021. [Online]. Available: https://doi.org/10.1155/2021/9936837

- [17] Q. Wu, J. Xu, Y. Zeng, D. W. K. Ng, N. Al-Dhahir, R. Schober, and A. L. Swindlehurst, "A comprehensive overview on 5G-and-beyond networks with UAVs: From communications to sensing and intelligence," *IEEE Journal on Selected Areas in Communications*, pp. 1–1, 2021.
- [18] C.-W. Hsu, Y.-L. Hsu, and H.-Y. Wei, "Energy-efficient edge offloading in heterogeneous industrial IoT networks for factory of future," *IEEE Access*, vol. 8, pp. 183 035–183 050, 2020.
- [19] T. N. Weerasinghe, V. Casares-Giner, I. A. M. Balapuwaduge, and F. Y. Li, "Priority enabled grant-free access with dynamic slot allocation for heterogeneous mMTC traffic in 5G NR networks," *IEEE Transactions on Communications*, vol. 69, no. 5, pp. 3192–3206, 2021.
- [20] N. Ansari, Q. Fan, X. Sun, and L. Zhang, "SoarNet," Wireless Commun., vol. 26, no. 6, p. 37–43, Dec. 2019. [Online]. Available: https://doi.org/10.1109/MWC.001.1900126
- [21] M. A. Hossain, A. R. Hossain, and N. Ansari, "Numerology-capable UAV-MEC for future generation massive IoT networks," *IEEE Internet* of Things Journal, vol. 9, no. 23, pp. 23860–23868, 2022.
- [22] Y. Yin, M. Liu, G. Gui, H. Gacanin, H. Sari, and F. Adachi, "Cross-layer resource allocation for UAV-Assisted wireless caching networks with NOMA," *IEEE Transactions on Vehicular Technology*, vol. 70, no. 4, pp. 3428–3438, 2021.
- [23] H. Tadayyoni, M. H. Ardakani, A. R. Heidarpour, and M. Uysal, "Ultraviolet communications for unmanned aerial vehicle networks," *IEEE Wireless Communications Letters*, vol. 11, no. 1, pp. 178–182, 2022
- [24] A. Alzidaneen, A. Alsharoa, and M.-S. Alouini, "Resource and placement optimization for multiple UAVs using backhaul tethered balloons," *IEEE Wireless Communications Letters*, vol. 9, no. 4, pp. 543–547, 2020.
- [25] A. Al-Hourani, S. Kandeepan, and A. Jamalipour, "Modeling air-to-ground path loss for low altitude platforms in urban environments," in 2014 IEEE Global Communications Conference, 2014, pp. 2898–2904.
- [26] D. Tse and P. Viswanath, Fundamentals of Wireless Communication. USA: Cambridge University Press, 2005.
- [27] W. Liu, L. Zhang, and N. Ansari, "Laser charging enabled DBS placement for downlink communications," *IEEE Transactions on Network Science and Engineering*, vol. 8, no. 4, pp. 3009–3018, 2021.
- [28] S. Rajagopal, S. Abu-Surra, and M. Malmirchegini, "Channel feasibility for outdoor Non-Line-of-Sight mmWave mobile communication," in 2012 IEEE Vehicular Technology Conference (VTC Fall), 2012, pp. 1–6.
- [29] W. Khawaja, O. Ozdemir, and I. Guvenc, "UAV air-to-ground channel characterization for mmWave systems," in 2017 IEEE 86th Vehicular Technology Conference (VTC-Fall), 2017, pp. 1–5.
- [30] R. Ali, Y. B. Zikria, A. K. Bashir, S. Garg, and H. S. Kim, "URLLC for 5G and beyond: Requirements, enabling incumbent technologies and network intelligence," *IEEE Access*, vol. 9, pp. 67064–67095, 2021.



Mohammad Arif Hossain (S'19) received the B.Sc. degree in Electrical and Electronic Engineering from Khulna University of Engineering and Technology, Khulna, Bangladesh and the M.Sc. degree in Electronics Engineering from Kookmin University, Seoul, South Korea. He is currently pursuing the Ph.D. degree in Computer Engineering at the New Jersey Institute of Technology, Newark, NJ, USA. He has (co-)authored forty journal and conference publications. His current research interests include cloud and edge computing, NOMA, network slicing,

network optimization, and machine learning.



Nirwan Ansari (S'78, M'83, SM'94, F'09), Distinguished Professor of Electrical and Computer Engineering at the New Jersey Institute of Technology (NJIT), received his Ph.D. from Purdue University, MSEE from the University of Michigan, and BSEE (summa cum laude with a perfect GPA) from NJIT. He is also a Fellow of National Academy of Inventors. He has published three books and (co-)authored 700 technical publications, over half published in widely cited journals/magazines. He has guest-edited numerous special issues covering various emerging

topics in communications and networking. He is the Editor-in-Chief of IEEE Wireless Communications Magazine and has served on the editorial/advisory board of over ten journals. His current research focuses on green communications and networking, cloud computing, drone-assisted networking, and various aspects of broadband networks. He was elected to serve in the IEEE Communications Society (ComSoc) Board of Governors as a member-atlarge, has chaired some ComSoc technical and steering committees, is current Director of ComSoc Educational Services Board, has been serving in many committees such as the IEEE Fellow Committee, and has been actively organizing numerous IEEE International Conferences/Symposia/Workshops. Some of his recognitions include several excellence in teaching awards, a few best paper awards, NCE Excellence in Research Award, several ComSoc TC technical recognition awards, NJ Inventors Hall of Fame Inventor of the Year Award, Thomas Alva Edison Patent Award, Purdue University Outstanding Electrical and Computer Engineering Award, NCE 100 Medal, NJIT Excellence in Research Prize and Medal, and designation as a COMSOC Distinguished Lecturer. He has also been granted more than 40 U.S. patents.



Abdullah Ridwan Hossain (S'20) received the B.E and M.S degrees in Electrical Engineering from The City College of New York, City University of New York, New York, NY, in 2017 and 2019, respectively. He is currently pursuing his Ph.D. degree in Electrical Engineering at the New Jersey Institute of Technology, Newark, NJ. He has (co)authored twelve journal publications as well as three book chapters. His research interests include machine learning, free space and fiber optics, optimization of optical, wireless, core networks, and

UAV communications, as well as accreditation and assessment.